Iranian Journal of Materials Forming

Research Article

Plastic Deformation of Nano-Single Crystal Co-Cr-Ni- Fe-Mn High Entropy Alloy in Tension From 10 K to 1000 K by Atomistic Simulations

R. Mohammadzadeh* and A. Heidarzadeh

Department of Materials Engineering, Azarbaijan Shahid Madani University, Tabriz, Iran

ARTICLE INFO

ABSTRACT

The plastic deformation behavior of nano-single crystals of the equiatomic CoCrNiFeMn high entropy alloy (HEA) with the face-centered cubic structure has been studied in tension as a function of temperature from 10 K to 1000 K using atomistic simulations. It was found that the critical stress for the slip was decreased with the increase in temperature. The results showed that the temperature had a substantial effect on the deformation mechanism. Intrinsic stacking faults and dislocations observed extensively at 10 K but not substantially at a temperature of 1000 K. Plastic deformation at a temperature of 10 K has occurred by means of partial dislocations slip whereas slip and amorphization is observed at 1000 K.

1. Introduction

As new classes of materials, high entropy alloys (HEAs) have attracted great consideration in recent years due to their interesting mechanical properties at extreme conditions [1-5]. There is an increasing interest in the development of new non-equiatomic HEAs with high ductility and strength by adding secondary/tertiary phases in HEAs [6-9]. However, the CoCrNiFeMn HEA with equiatomic composition and the fcc (face-centered cubic) structure, initially found by Cantor et al. [10], is still a functional alloy. Because the ductility and tensile strength of equiatomic CoCrNiFeMn HEA increases with a decrease in the temperature [11, 12]. It has also shown that the mechanical properties of HEAs strongly depend on their composition. For example, the

CoCrNiFeMn HEA undergoes an fcc to hcp (hexagonal-close-packed) phase transformation at pressures over 14 GPa [13]. The equiatomic CoCrNiFeMn HEA was reported to exhibit a fracture toughness of 200 MPa√m, tensile strength of 1 GPa, and tensile ductility above 7% at 77 K [14]. High fracture toughness at room temperature in CoCrNiFeMn HEA has been described due to the slip of partial dislocations, formation of stacking fault and nano twins across the crack tip [15]. These results show that the good mechanical properties of HEAs should mainly be caused due to the activation of several plastic deformation mechanisms.

To determine and quantify the role of various microstructural parameters, like the grain size, stacking fault energy and dislocation density to the mechanical response of HEAs, systematic experiments on small-

---

scale HEA samples should be conducted. Small-scale experiments are also helpful for the design of nano/micro electromechanical systems [16]. In addition to exploring microstructural parameters, investigating the effect of temperature on the deformation behavior of HEAs is also required for satellite parts, tanks for liquefied gases, and aerospace applications.

To avoid grain size effects, there is a crucial need for experimental data of single crystal HEAs from which the micro/nano structural evolution and twinning stress can be derived. There are a few reports on the yield strength and twinning stress of single crystals of the CoCrNiFeMn HEA [17, 18]. Kireeva et al. [17] measured the twinning stress in the single crystalline CoCrFeMnNi HEA and determined shear stress values for twinning in the range of 110-140 MPa at room temperature, which are considerably lower than the value (~235 MPa) evaluated from the twinning stress of polycrystalline HEA divided by the Taylor factor [16]. Kawamura et al. [18] investigated the plastic deformation behavior of single crystals of CoCrNiFeMn HEA experimentally and reported that the critical resolved shear stress for {111} <110> slip was decreased by increasing temperature.

Additional studies are needed to promote the fundamental understanding of the deformation behavior of CoCrNiFeMn HEA at low and high temperatures. Molecular dynamics (MD) simulation can give an extensive knowledge on the atomic structural evolution, which is difficult to be obtained experimentally [19]. In the present study, we investigate the plastic deformation behavior of nano-single crystals of equiatomic CoCrNiFeMn HEA in tension at temperatures of 10, 600 and 100 K by MD simulations to answer some of the open-ended questions.

2. Materials and Methods

MD is an atomistic approach to provide the trajectories of systems with a lot of atoms via numerical integration of Newton's equations of motion, with a correct description of the boundary conditions, initial conditions, and interatomic potential. In classical MD

simulation, the position of atoms derived from their initial positions $(\vec{r}_0, \vec{v}_0)$ based on Newton's equation of motion are illustrated as follows:

$$\frac{d^2\vec{r}_i}{dt^2} = \frac{\vec{F}_i}{m_i} \tag{1}$$

Where $\vec{v}_i$ is the velocity, $\vec{r}_i$ is the position, and m_i is the mass of atom i. In the lack of external force fields, the force $\vec{F}_i$, can be obtained as the gradient of the potential of system for atomic movement by

$$\vec{F}_i = -\vec{\nabla}_{i\phi}(\vec{r}_1, \vec{r}_2, \vec{r}_3, \ldots, \vec{r}_N) \tag{2}$$

Where, $\phi(\vec{r}_1, \vec{r}_2, \vec{r}_3, \ldots, \vec{r}_N)$ illustrates the potential energy of the system in specific arrangement of atoms. After constructing the required structures, specifying interatomic potentials, and giving initial position and velocity of atoms, MD enables the system of interest to evolve according to a defined time integration algorithm and ensembles. The MD simulations in this study were performed on the single crystalline equiatomic CoCrNiFeMn HEA with fcc structure and lattice constant of 3.595 Å as shown in Fig. 1. The dimension of single crystals was 12.3×12.4×10.1 nm³ which contained approximately 134400 atoms. The orientation of single crystal HEAs along x, y and z were [11$\bar{2}$], [111], and [1$\bar{1}$0], respectively. Periodic boundary conditions were applied in three directions. All simulations were carried out with the open-source LAMMPS code [20] by use of CoCrNiFeMn interatomic potential which was developed by Choi et al. [21]. The interactions of Co, Cr, Ni, Fe, and Mn atoms were explained with a modified embedded atom method (MEAM) expression in which the total energy of the system is determined by Eq. (3) [21].

$$E = \sum_i \left[F_i(\bar{\rho}_i) + \frac{1}{2} \sum_{i \neq j} \phi_{ij}(r_{ij}) \right] \tag{3}$$

Where F_i is the embedding energy function for atom i embedded in a background electron density $\bar{\rho}_i$, and $\phi_{ij}(r_{ij})$
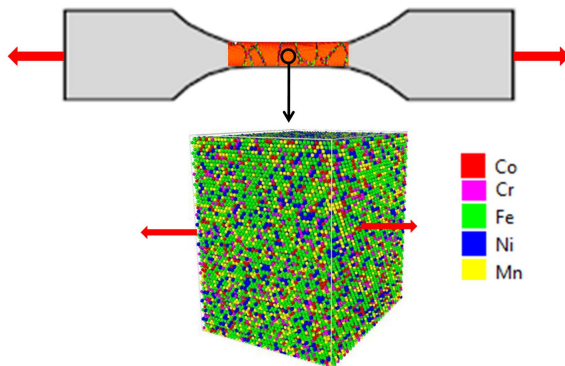
Fig. 1. Schematic diagram of the uniaxial tensile test specimen and nano-single crystalline CoCrNiFeMn HEA sample used for MD simulations, the red arrows indicate the tensile loading direction.

is the pair potential interaction between atoms *i* and *j* separated by a distance r_{ij}. Interatomic potential presented by [21] has been validated with random distribution of the Co, Cr, Ni, Fe, and Mn elements at 10, 600 and 1000 K. The results showed an equilibrium phase with fcc structure at these temperatures.

To minimize energy, the initial structures firstly were relaxed using a conjugate gradient procedure with force tolerance of 10^{-6} and energy tolerance of 10^{-7}. Then, a velocity profile was assigned to the simulated samples according to the simulation temperature of 10 K, 600 K, or 1000 K. The single crystals were then equilibrated at the given temperature for 150 ps under zero pressure using microcanonical ensemble (NVE) as time integration scheme. All simulations were carried out with time step of 1 fs. Tensile tests were performed through deformation of the simulation boxes up to a total strain of 13% at a strain rate of 10^9 s^{-1} under the isothermal-isobaric (NPT) ensemble. Such a high strain rate is an unavoidable effect of the time scales obtainable during MD simulations and will overestimate the yield stress in HEA samples. We thus limit our discussion of the MD simulations to the qualitative comparison. Statistical analysis and visualization of crystal structures and defects were accomplished by OVITO software [22]. Common neighbor analysis (CNA) and Dislocation Extraction Algorithm (DXA) were applied to determine lattice structure and dislocations [22]. To provide a local crystal structure to an atom, three typical numbers are

computed by CNA for each of the N neighbor bonds of the central atom: i) the number of neighbor atoms of the central atom and its bonded neighbor have in common; ii) the total number of bonds between these common neighbors; and iii) the number of bonds in the longest chain of bonds connecting the common neighbors. This yields N triplets, which are compared to a set of reference signatures to assign a structural type to the central atom (Table 1). OVITO gives a list of optimal cutoff distances for bcc, hcp and fcc crystal structures formed by common pure elements. The structural type identified by the algorithm is encoded as an integer value (1= fcc, face-centered cubic, 2= hcp, hexagonal close-packed, 3= bcc, body-centered cubic, 4= ico, icosahedral coordination and 0= other, unknown coordination or amorphous structure). The DXA approach is based on the calculation of the incompatible elastic displacement field around dislocations that requires mapping bond vectors from the distorted atomic configuration to strain-free reference configuration. The fundamental approach based on the DXA is the Burgers circuit construction, which is the accepted method, proposed in the 1950s, to distinguish dislocations from other crystal defects and discover their Burgers vectors.

Table 1. CNA signatures of common crystal structures. An fcc coordinated atom has twelve bonds of (421) type. That is, any two near-neighbors in an fcc crystal have exactly four common neighbors, which are interconnected by two bonds. And the longest continuous chain these two bonds form is of length one

fcc (N=12)	hcp (N=12)	bcc (N=14)	Cubic diamond (N=16)
12×(421)	6×(421) 6×(422)	8×(666) 6×(444)	12×(543) 4×(663)

3. Results

3.1. Temperature dependence of tensile deformation behavior

Stress-strain curves of HEA single crystals deformed at 10, 600, and 1000 K are shown in Fig. 2. For all simulated samples, tensile stress values increase linearly with strain in a small regime of engineering strain. Then, the stress drops in all stress-strain curves, as shown in Fig. 2. This maximum stress shows the required stress for homogeneous nucleation of dislocation, which decreases
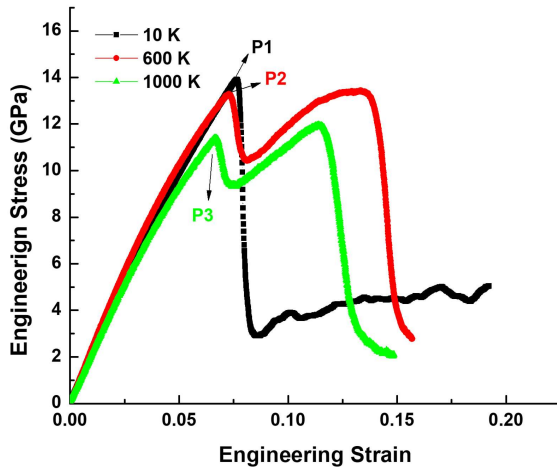
Fig. 2. Representative tensile stress-strain curves of simulated single crystalline HEA at 10 K, 600 K, and 1000 K.

by increasing the temperature from 10 K to 1000 K. The peak stresses for samples at temperatures of 10 K, 600 K, and 1000 K are 5.59, 4.83, 3.68, and 2.85 GPa, which are denoted by P1, P2, and P3, respectively. At high temperatures the lattice has a higher vibration amplitude of atoms in comparison with that at low temperatures. Therefore, the atomic bonds can break readily at high temperature, which results in a lower stress for nucleation of dislocations.

Local maximum stresses are observed in the stress-strain curves of HEA single crystals at a temperature of 600 K and 1000 K. We believe this is because of the crystalline to amorphous phase transformation at high temperatures. The details of this will be discussed later in section 3.2. The temperature dependence of mechanical properties of the single crystalline CoCrNiFeMn HEA identified by MD simulations in this study are very similar to single crystals of the CrMnFeCoNi HEA revealed by experimental methods [23]. However, the values of the critical resolved shear stress or yield stress are higher than those of experimental values on CrMnFeCoNi HEA [23]. This is because high strain rate and a perfect single crystal structure were applied in MD simulations.

3.2. Atomic structures

To better explore the plastic deformation mechanisms and phase transformation, the atomic structure of deformed samples was analyzed at different temperatures. The atomic configurations of tensile deformed samples at different temperatures and after the tensile strain of 6, 7, 8, 9, 10, 11, 12, and 13% are shown in Figs. 3-5.
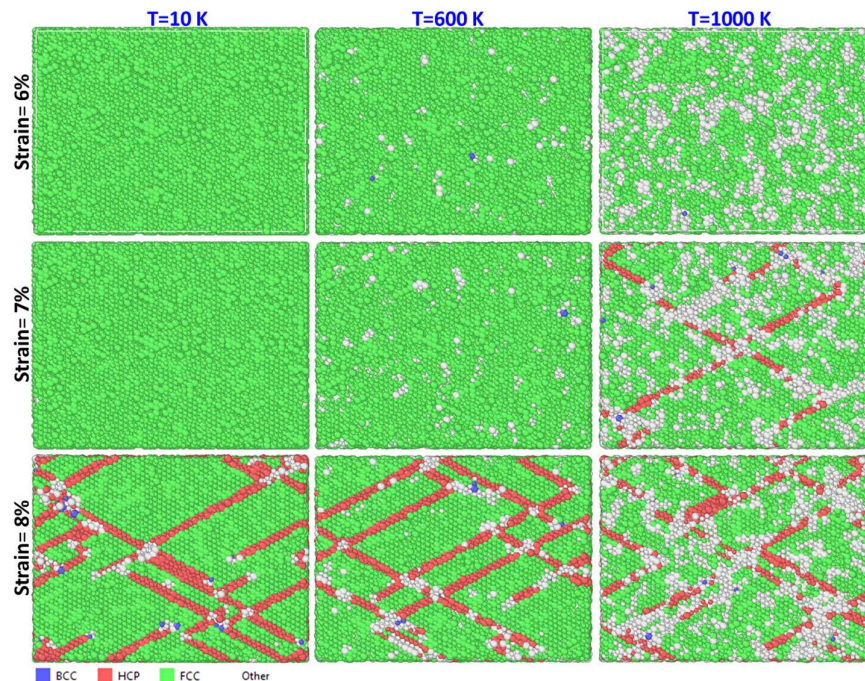

Fig. 3. Atomic structure evolution of simulated single crystalline HEA tensile deformed to an axial strain of 6, 7, 8% at 10 K, 600 K and 1000 K. Atoms were colored according to CNA parameter. The green and red atoms represent the fcc and hcp crystal structures, respectively, and the white for other atoms.
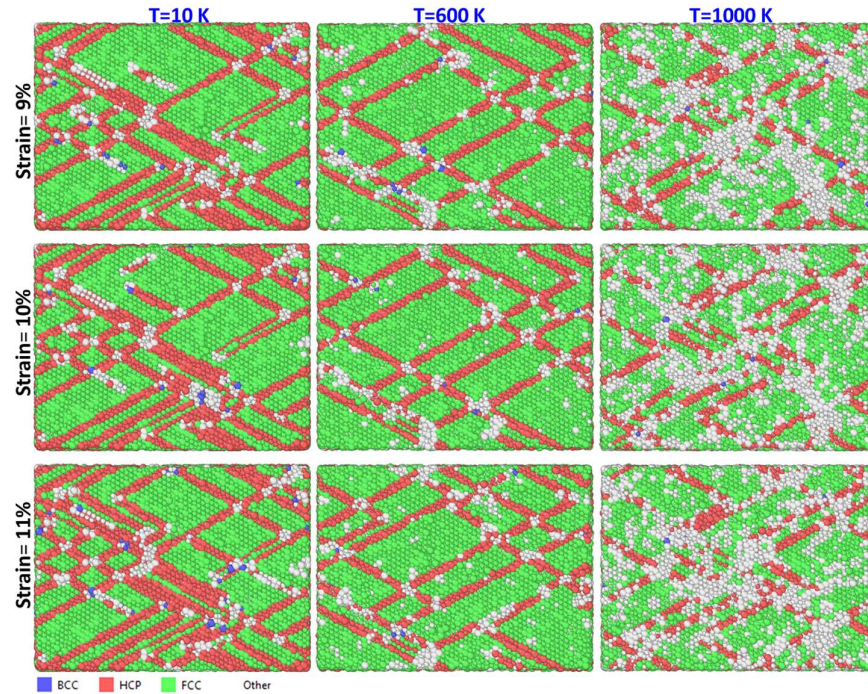
Fig. 4. Atomic structure evolution of simulated single crystalline HEA tensile deformed to an axial strain of 9, 10, 11% at 10 K, 600 K and 1000 K. Atoms were colored according to CNA parameter. The green and red atoms represent the fcc and hcp crystal structures, respectively, and the white for other atoms.

Atoms in hcp (hexagonal close-packed) structure are colored red, fcc (face centered cubic) atoms are colored in green, and atoms with undefined atomic structures or amorphous structures are shown in white. At all temperatures, the plastic deformation is dominated by intrinsic stacking faults (ISFs) which composed of layers of atoms with hcp structure.

At the strain of 6%, as seen in Fig. 3, that amorphous phase formed as other atoms with no special structure (shown as white atoms in Fig. 3) at a temperature of 600 and 1000 K. By increasing strain from 6 to 7%, ISFs were nucleated in the HEA sample with a temperature of 10 K. At the strain of 8%, ISFs mainly nucleated and grew at all temperature levels. As it can be seen in Figs. 3 and 4, as the strain increases from 9 to 13%, many ISFs were activated in the single crystal HEA at low temperature in
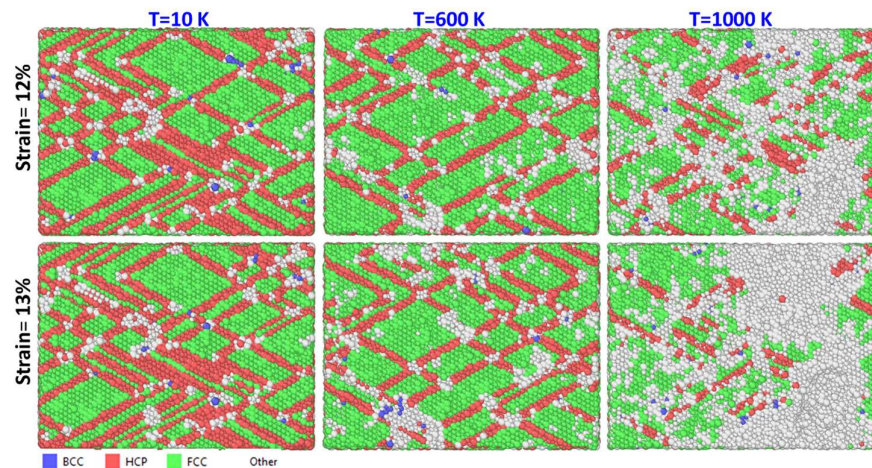

Fig. 5. Atomic structure evolution of simulated single crystalline HEA tensile deformed to an axial strain of 12 and 13% at 10 K, 600 K and 1000 K. Atoms were colored according to CNA parameter. The green and red atoms represent the fcc and hcp crystal structures, respectively, and the white for other atoms.

comparison to that of high temperatures.

To determine quantitatively the structural changes in different temperatures, the CNA analysis was performed to characterize the volume fraction of fcc, hcp, and amorphous structures at various strain levels. The volume fraction of different crystalline or non-crystalline structures versus strain at a temperature of 10, 600 and 1000 K are shown in Fig. 6. It is evident from
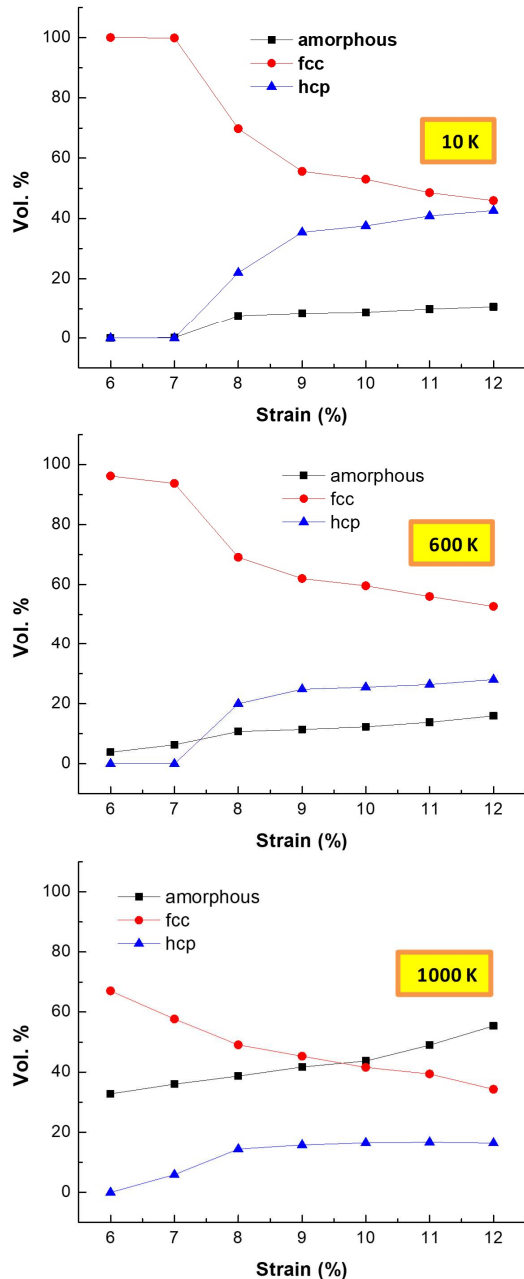
Fig. 6 that the volume fraction of atoms with hcp structure decreases from 37.5% at 10 K to 25.5% at 600 K at strain level of 10%. This is consistent with the experimental results obtained by Stepanov et al. [24] on the microstructure evolution of polycrystalline CoCrFeNiMn HEA during rolling at 77 K and 293 K. Stepanov et al. [24] reported that plastic deformation at 77 K and 293 K accompanied by twinning and the fraction of twinned grains at a temperature of 77 K was more extensive than 293 K. Also, this result is in accordance with the experimental work of Zhao et al. [25]. They showed that at high strain rates and/or strains, deformation mechanism exhibits itself, that of solid-state amorphization (see Fig. 7). The volume fraction of amorphous structure at 10 K is slightly increased with strain from 0.1% at a strain of 7% to 10.6% at a strain of 12%. However, at 600 K and 1000 K, under the strain range of 7-12%, the volume fraction of amorphous structure increases significantly from 6.3 to 15.9 and from 36 to 55.4%, respectively. This result may suggest that high temperature deformation causes a phase transformation from crystalline to amorphous structure in nano crystalline HEA.

3.3. Dislocation structures

Typical dislocation structures recognized in simulated nano-single crystals of CoCrNiFeMn HEA deformed in tension to plastic strain of 7, 8, 9, 10, 11, 12% at 10, 600 and 1000 K are shown in Figs. 8 and 9. In these figures, dislocations appear as blue colored lines and areas where
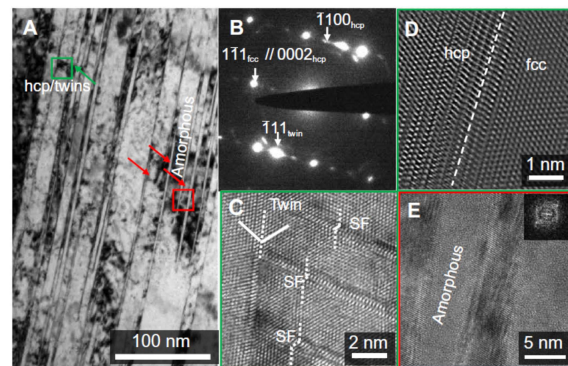

Fig. 6. Volume fraction of hcp, fcc and amorphous phases present in the dynamically deformed specimens as a function of total strain at temperature of 10 K, 600 K and 100 K.

Fig. 7. Deformation structure of the CrMnFeCoNi HEA subjected to extreme deformation. (A) Bright-field TEM image and (E) High-resolution image of the amorphous bands (red square in (A)) [25].
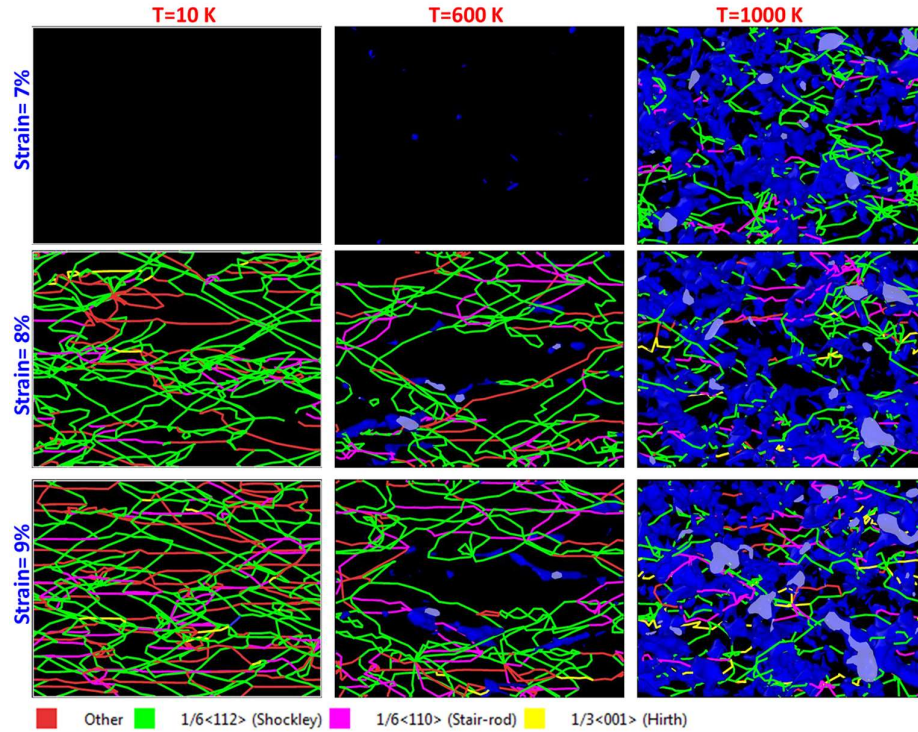
Fig. 8. Distribution of dislocation and defects in single crystalline HEA at temperatures of 10 K, 600 k and 100 K under strain levels of 7, 8 and 9 %. The lines with different colors expressed various types of dislocations, where green, blue, pink and yellow denoted the Shockley 1/6 < 112 >, Perfect 1/2 < 110 >, Srair-rod 1/6 < 110 > and Hirth 1/3 < 001 > dislocations. Red lines are the dislocations that cannot be identified by DXA. The blue meshes are the defects meshes
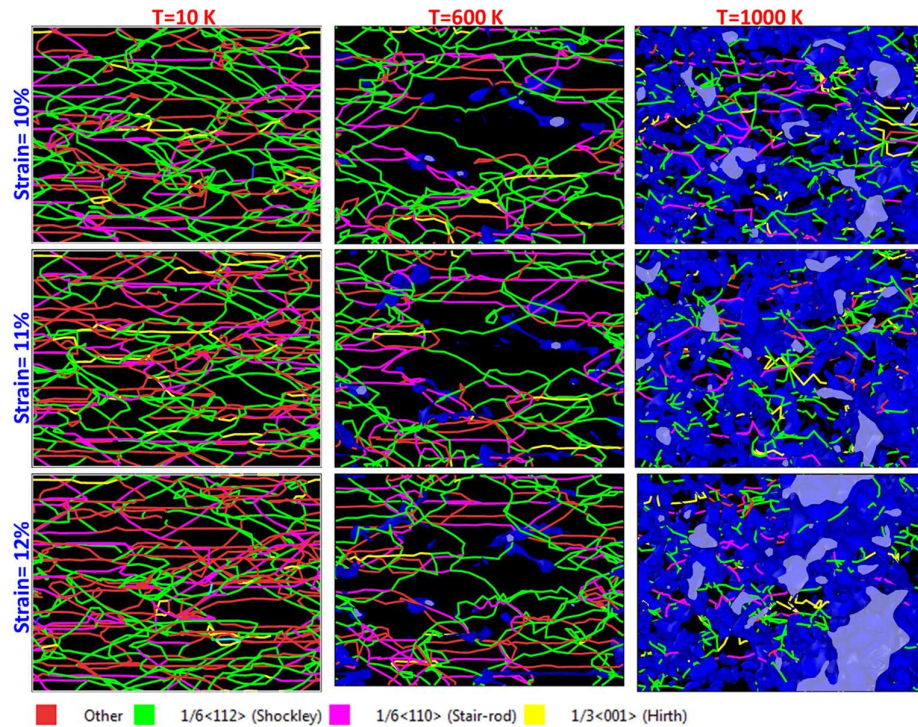

Fig. 9. Distribution of dislocation and defects in single crystalline HEA at temperatures of 10 K, 600 k and 100 K, at strain levels of 10, 11 and 12 %. The lines with different colors express various types of dislocations, where green, blue, pink and yellow denotes the Shockley 1/6 < 112 >, Perfect 1/2 < 110 >, Srair-rod 1/6 < 110 > and Hirth 1/3 < 001 > dislocations. Red lines are the dislocations that cannot be identified by DXA. The blue meshes are the defects meshes.

no lattice/crystal matching could be resolved. One can see that at total strain of 7%, nano single crystalline HEA at a temperature of 1000 K has a higher network of dislocations and defect mesh, while no dislocations could be detected at 10 K and 600 K. Indeed, widely separated dislocations can be visible at 10 K and 600 K when strain increases to 8%. As expected, the dislocations in the single crystals are of the Shockley partial types with Burgers vector of $\frac{1}{6} < 112 >$. Additionally, one typical dislocation reaction product, stair-rod sessile dislocation with Burger vectors of $\frac{1}{6} < 110 >$ (Lomer–Cottrell lock), can be observed in Fig. 8. The sessile dislocations cannot move along the original slip plane and are pinned inside the crystal, and they hinder dislocation movement. The dislocation evolution was found to vary depending on the deformation temperature. By increasing the plastic strain, more dislocations are nucleated, and growth occurs at temperatures of 10 and 600 K, as shown in Figs. 8 and 9. However, at high temperatures of 1000 K, amorphization also assists the plasticity.

Fig. 9 shows that HEA sample, which deformed at 10 K, contained a high density of dislocations. The average dislocation density of all samples during tensile straining are shown in Fig. 10. At temperatures of 10 K and 600 K, the total length of dislocations increases by increasing strain from 7% to 12%. At strain range of 8-12%, the total length of dislocations during plastic deformation at 10 K remained at a high level and reached more than 1000 nm. While the average length of total dislocations at 1000 K was stable and kept at a relatively low level of 425 nm during tensile straining from 7% to 12%, as shown in Fig. 9.

4. Discussion

In Figs. 4 and 5, the final lengths of intrinsic SFs are different. At both 600 K and 1000 K, the growth lengths of SFs decrease, although this is more obvious at 1000 K. The most remarkable observation in this study is the formation of nanoscale amorphous regions in HEAs upon tensile deformation at high temperatures, which has not been reported previously. The amorphous parts can provide strong barriers for the motion of dislocations
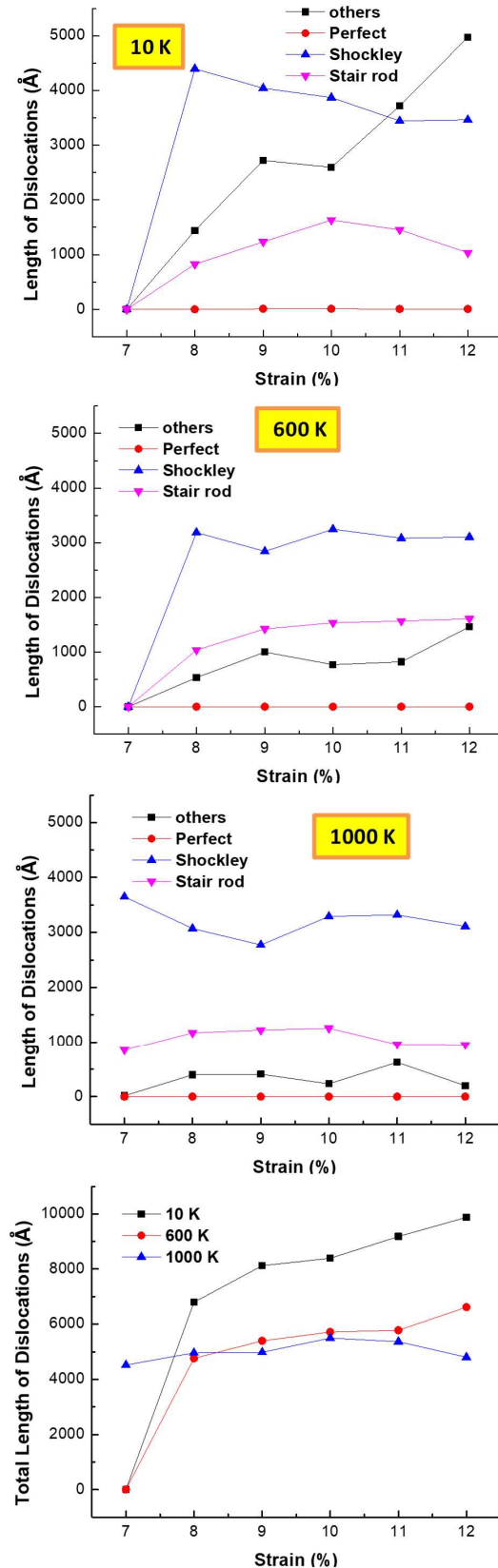

Fig. 10. Length of different types of dislocations in the dynamically deformed specimens as a function of total strain at temperature of 10 K, 600 K, and 1000 K.

and propagation of intrinsic SFs/nano-twins, resulting in a substantial strengthening effect. The chemical composition of the matrix with an fcc structure was compared with that of the amorphous bands and no distinct composition difference between matrix and amorphous regions was detected. Therefore, the crystalline to amorphous transition in present HEA can be regarded as a solid-state amorphization. Crystalline to amorphous transition is extensively observed in almost ceramics, covalent pure elements, and intermetallic compounds [26]. Various mechanical techniques can amorphize crystalline materials partially or fully, including severe plastic deformation, mechanical alloying, and irradiation with ions or electrons [27, 28]. From the perspective of the thermodynamic driving force, amorphization takes place when the free energy of the amorphous is lower than that of the crystalline phase. Crystalline to amorphous transition in the studied HEA upon tensile deformation at high temperatures may be caused due to the significant accumulation of dislocations inside shear regions. As shown in Fig. 8, the accumulation of dislocations in the strain level of 7% at 1000 K is much faster than 10 K and 600 K, suggesting that the severe strain induced by accumulation of dislocations in shear regions. As the accumulation of dislocations in constrained shear regions increases the free energy of original fcc matrix to a point higher than that of amorphous structure, energy difference should drive amorphization.

5. Conclusion

In spite of several studies on the deformation behavior of CoCrNiFeMn HEA, its structural evolution at nanoscale at different temperatures remains unrevealed. In this study, the plastic deformation mechanism of nano-single crystalline CoCrNiFeMn HEA under tensile deformation at various temperatures is investigated via MD simulations, in terms of atomic structure evolution, stress-strain relationship and dislocation evolution. Atomistic simulation results showed that perfect dislocations with burger vectors of $\frac{1}{2} < 110 >$ dissociated into Shockley partial dislocations

with burger vectors of $\frac{1}{6} < 112 >$ and the critical shear stress for the slip of partial dislocations increased by decreasing temperature. The dislocation density is higher at 10 K, which results in relatively smooth deformation and stress-strain curves. At low temperatures of 10 K and 600 K, the interaction of stacking faults and partial dislocations causes Lomere-Cottrel lock. Crystalline to amorphous phase transformation dose occur at 1000 K at a strain of 7%, but it does not form at 10 K. A very high fraction of the amorphous regions form during tensile deformation at a temperature of 1000 K and its volume fraction increases by increasing the strain. As a result, the stress in the nano-single crystal HEA at 1000 K changes in a zigzag type with an increase in strain. This study could provide an atomic-scale understanding of the deformation mechanisms of nano-single crystalline CoCrNiFeMn HEA at low and high temperatures, which can give guidance for future developments of high entropy alloys.

6. References

[1] R. Feng, C. Zhang, M.C. Gao, Z. Pei, F. Zhang, Y. Chen, D. Ma, K. An, J.D. Poplawsky, L. Ouyang, Y. Ren, High-throughput design of high-performance lightweight high-entropy alloys, *Nature Communications*, 12(1) (2021) 1-10.

[2] Y. Wu, F. Zhang, X. Yuan, H. Huang, X. Wen, Y. Wang, M. Zhang, H. Wu, X. Liu, H. Wang, S. Jiang, Short-range ordering and its effects on mechanical properties of high-entropy alloys, *Journal of Materials Science & Technology*, 62 (2021) 214-220.

[3] M. Klimova, D. Shaysultanov, A. Semenyuk, S. Zherebtsov, N. Stepanov, Effect of carbon on recrystallised microstructures and properties of CoCrFeMnNi-type high-entropy alloys, *Journal of Alloys and Compounds*, 851 (2021) 156839.

[4] Q.F. He, P.H. Tang, H.A. Chen, S. Lan, J.G. Wang, J.H. Luan, M. Du, Y. Liu, C.T. Liu, C.W. Pao, Y. Yang, Understanding chemical short-range ordering/demixing coupled with lattice distortion in solid solution high entropy alloys, *Acta Materialia*, 216 (2021) 117140.

[5] R. Gawel, Ł. Rogal, J. Dąbek, M. Wójcik-Bania, K. Przybylski, High temperature oxidation behaviour of non-equimolar AlCoCrFeNi high entropy alloys, *Vacuum*, 184 (2021) 109969.

[6] R.K. Nutor, Q.P. Cao, X.D. Wang, D.X. Zhang, J.Z. Jiang, Tunability of the mechanical properties of (Fe50Mn27Ni10Cr13) 100-xMox high-entropy alloys via secondary phase control, *Journal of Materials Science & Technology*, 73 (2021) 210-217.

[7] H.C. Liu, C.W. Tsai. Effect of Ge addition on the microstructure, mechanical properties, and corrosion behavior of CoCrFeNi high-entropy alloys, *Intermetallics*, 132 (2021) 107167.

[8] P.P. Cao, H. Wang, J.Y. He, C. Xu, S.H. Jiang, J.L. Du, X.Z. Cao, E.G. Fu, Z.P. Lu, Effects of nanosized precipitates on irradiation behavior of CoCrFeNi high entropy alloys, *Journal of Alloys and Compounds*, 859 (2021) 158291.

[9] İ.B.A. Şimşek, M.N. Arık, Ş. Talaş, A. Kurt, The effect of B addition on the microstructural and mechanical properties of FeNiCoCrCu high entropy alloys, *Metallurgical and Materials Transactions A,* 52(5) (2021) 1749-1758.

[10] B. Cantor, I.T.H. Chang, P. Knight, A.J.B. Vincent, Microstructural development in equiatomic multicomponent alloys, *Materials Science and Engineering: A*, 375 (2004) 213-218.

[11] S.J. Sun, Y.Z. Tian, X.H. An, H.R. Lin, J.W. Wang, Z.F. Zhang, Ultrahigh cryogenic strength and exceptional ductility in ultrafine-grained CoCrFeMnNi high-entropy alloy with fully recrystallized structure, *Materials Today Nano*, 4 (2018) 46-53.

[12] S.H. Joo, H. Kato, M.J. Jang, J. Moon, C.W. Tsai, J.W. Yeh, H.S. Kim, Tensile deformation behavior and deformation twinning of an equimolar CoCrFeMnNi high-entropy alloy, *Materials Science and Engineering: A*, 689 (2017) 122-133.

[13] C.L. Tracy, S. Park, D.R. Rittman, S.J. Zinkle, H. Bei, M. Lang, R.C. Ewing, W.L. Mao, High pressure synthesis of a hexagonal close-packed phase of the high-entropy alloy CrMnFeCoNi, *Nature communications*, 8(1) (2017) 1-6.

[14] B. Gludovatz, A. Hohenwarter, D. Catoor, E.H. Chang, E.P. George, R.O. Ritchie, A fracture-resistant high-entropy alloy for cryogenic applications, *Science*, 345(6201) (2014) 1153-1158.

[15] Z. Zhang, M.M. Mao, J. Wang, B. Gludovatz, Z. Zhang, S.X. Mao, E.P. George, Q. Yu, R.O. Ritchie, Nanoscale origins of the damage tolerance of the high-entropy alloy CrMnFeCoNi, *Nature communications*, 6(1) (2015) 1-6.

[16] S.W. Lee, Y. Cheng, I. Ryu, J.R. Greer, Cold-temperature deformation of nano-sized tungsten and niobium as revealed by in-situ nano-mechanical experiments, *Science China Technological Sciences*, 57(4) (2014) 652-662.

[17] I.V. Kireeva, Y.I. Chumlyakov, Z.V. Pobedennaya, I.V. Kuksgausen, I. Karaman, Orientation dependence of twinning in single crystalline CoCrFeMnNi high-entropy alloy, *Materials Science and Engineering: A*, 705 (2017) 176-181.

[18] M. Kawamura, M. Asakura, N.L. Okamoto, K. Kishida, H. Inui, E.P. George, Plastic deformation of single crystals of the equiatomic Cr− Mn− Fe− Co− Ni high-entropy alloy in tension and compression from 10 K to 1273 K, *Acta Materialia*, 203 (2021) 116454.

[19] O.R. Deluigi, R.C. Pasianot, F.J. Valencia, A. Caro, D. Farkas, E.M. Bringa, Simulations of primary damage in a High Entropy Alloy: Probing enhanced radiation resistance, *Acta Materialia*, 213 (2021) 116951.

[20] A.P. Thompson, H.M. Aktulga, R. Berger, D.S. Bolintineanu, W.M. Brown, P.S. Crozier, P.J. in't Veld, A. Kohlmeyer, S.G. Moore, T.D. Nguyen, R. Shan, LAMMPS-A flexible simulation tool for particle-based materials modeling at the atomic, meso, and continuum scales, *Computer Physics Communications*, 271 (2022) 108171.

[21] W.M. Choi, Y.H. Jo, S.S. Sohn, S. Lee, B.J. Lee, Understanding the physical metallurgy of the CoCrFeMnNi high-entropy alloy: an atomistic simulation study, *npj Computational Materials*, 4(1) (2018) 1-9.

[22] A. Stukowski, Visualization and analysis of atomistic simulation data with OVITO–the Open Visualization Tool, *Modelling and Simulation in Materials Science and Engineering*, 18(1) (2009) 015012.

[23] M. Kawamura, M. Asakura, N.L. Okamoto, K. Kishida, H. Inui, E.P. George, Plastic deformation of single crystals of the equiatomic Cr− Mn− Fe− Co− Ni high-entropy alloy in tension and compression from 10 K to 1273 K, *Acta Materialia*, 203 (2021) 116454.

[24] N. Stepanov, M. Tikhonovsky, N. Yurchenko, D. Zyabkin, M. Klimova, S. Zherebtsov, A. Efimov, G. Salishchev, Effect of cryo-deformation on structure and properties of CoCrFeNiMn high-entropy alloy, *Intermetallics*, 59 (2015) 8-17.

[25] S. Zhao, Z. Li, C. Zhu, W. Yang, Z. Zhang, D.E. Armstrong, P.S. Grant, R.O. Ritchie, M.A. Meyers, Amorphization in extreme deformation of the CrMnFeCoNi high-entropy alloy, *Science advances*, 7(5) (2021) eabb3108.

[26] P.R. Okamoto, N.Q. Lam, L.E. Rehn, Physics of crystal-to-glass transformations, *solid state physics*, 52 (1999) 1-35.

[27] R.V. Sundeev, A.M. Glezer, A.V. Shalimova, Phase transformations «Amorphization↔ Crystallization» in metallic materials induced by severe plastic deformation, *Reviews on advanced materials science*, 54(1) (2018) 93-105.

[28] S. Zhao, R. Flanagan, E.N. Hahn, B. Kad, B.A. Remington, C.E. Wehrenberg, R. Cauble, K. More, M.A. Meyers, Shock-induced amorphization in silicon carbide, *Acta Materialia*, 158 (2018) 206-213.